# Wood anomalies in resonant photonic quasicrystals

A. N. Poddubny*
*Ioffe Physical-Technical Institute RAS, 26 Polytekhnicheskaya St., RU-194021 St. Petersburg, Russia*
(Received 13 September 2010; published 8 February 2011)

A theory of light diffraction from a planar quasicrystalline lattice with resonant scatterers is presented. Rich structure, absent in the periodic case, is found in specular reflection spectra, and interpreted as a specific kind of Wood anomaly, characteristic of quasicrystals. The theory is applied to semiconductor quantum dots arranged in Penrose tiling.

DOI: 10.1103/PhysRevB.83.075106 PACS number(s): 42.70.Qs, 61.44.Br, 71.35.−y

## I. INTRODUCTION

The discovery of quasicrystals initiated new fields of research in solid-state photonics.[1,2] These deterministic objects allow Bragg diffraction of light, like conventional photonic crystals, but are not restricted by the requirement of periodicity, and thus can be more easily tailored to the desired optical properties. Such an extra degree of freedom is especially important for the control of light-matter interaction in resonant photonic structures,[3] where the constituent materials possess resonant excitations, like excitons or plasmons. For example, a one-dimensional polaritonic Fibonacci quasicrystal based on quantum-well excitons has been realized in Ref. 4, while the two-dimensional (2D) plasmonic deterministic aperiodic arrays of metallic nanoparticles have been fabricated in Ref. 5.

It is also known that the interaction of light waves with diffraction grating can lead to the so-called Wood anomalies in optical spectra.[6–9] They can be defined as rapid variations of the intensity of various diffracted spectral orders in certain narrow frequency bands.[6] Indeed, the incident plane wave can undergo either specular reflection or diffraction. The interference of these processes may result in intricate optical spectra. However, to the best of our knowledge, no systematic study of Wood anomalies in *quasicrystalline* gratings has been performed yet, although their high importance for light transmission through aperiodic arrays of holes in metallic thin films has been mentioned in Ref. 10. Here we consider light diffraction from the 2D resonant photonic quasicrystals and crystals made of quantum dots. The main results of our paper are summarized below:

(1) For the *periodic* quantum dot lattice tuned to the in-plane Bragg diffraction condition, the specular reflection spectrum is dominated by a single peak. A weakly resolved notch where reflectivity turns to zero is present at the wing of this peak and corresponds to the lattice Wood anomaly.

(2) In the *quasicrystalline* lattice, this notch is shifted and an additional structured peak emerges in the reflection spectrum. The second peak can be interpreted as a lattice Wood anomaly of novel type, absent in the periodic case.

The rest of the paper is organized as follows. In Sec. II we formulate the problem and outline the calculation technique. Section III presents approximate analytical results for the reflection coefficient. Results of analytical and numerical calculation are discussed in Sec. IV. Section V is reserved for conclusions.

## II. PROBLEM DEFINITION AND METHOD OF CALCULATION

The structure under consideration consists of quantum dots, arranged in the canonical Penrose tiling[2,11] in the $xy$ plane and embedded in the dielectric matrix. The incident wave propagates along the $z$ axis, see Fig. 1(a). The Penrose tiling shown in Fig. 1(b) has fivefold rotational symmetry and can be defined as follows. First we introduce the basis of five vectors

$$\boldsymbol{e}_n = \left[\cos\left(\frac{2\pi n}{5}\right), \sin\left(\frac{2\pi n}{5}\right)\right], \quad n = 1,\ldots,5.$$

Then five sets of equidistant parallel lines $\boldsymbol{r}_{n,j}$ are defined, each set normal to the corresponding vector $\boldsymbol{e}_n$: $\boldsymbol{r}_{n,j}\cdot\boldsymbol{e}_n = j + (2/5)$, where index $j$ accepts all integer values. Finally, each cell in the obtained grid, bounded by the lines $\boldsymbol{r}_{1,j_1},\boldsymbol{r}_{1,j_1+1},\ldots,\boldsymbol{r}_{5,j_5},\boldsymbol{r}_{5,j_5+1}$, is mapped to the point $\boldsymbol{r} = a_r\sum_{n=1}^{5} j_n\boldsymbol{e}_n$, belonging to the Penrose lattice with the rhombus side equal to $a_r$. Such an approach is termed as the dual multigrid technique.[12] It can be used to generate quasiperiodic lattices with arbitrary degrees of rotational symmetry. Other equivalent definitions of the Penrose tiling are based on the cut-and-project technique.[13] The lattice structure factor

$$f(\boldsymbol{q}) = \lim_{M\to\infty}\frac{1}{M}\sum_{j=1}^{M} e^{2i\boldsymbol{q}\boldsymbol{r}_j} = \sum_{h_1\ldots h_4} f_{\mathbf{G}}\delta_{2\boldsymbol{q}-\boldsymbol{G}_{h_1\ldots h_4}} \qquad (1)$$

is shown in Fig. 2. It consists of Bragg peaks at the 2D diffraction vectors $\boldsymbol{G}_{h_1\ldots h_4} = G^*\sum_{n=1}^{4} h_n\boldsymbol{e}_n$, where $G^* = 4\pi\tau^2/(5a_r)$ and $\tau = (\sqrt{5}+1)/2$ is the golden mean. The structure factor $f(q)$ has $C_{5v}$ rotational symmetry. It means that each diffraction vector with an absolute value $G > 0$ belongs either to the set of five vectors $G\boldsymbol{e}_n$ $(n = 1,\ldots,5)$ or to the opposite set $G\boldsymbol{e}_n$. Within each set the structure factors are identical. In what follows we will call each such set a "star" of diffraction vectors. Since $f_{-\mathbf{G}} = f_{\mathbf{G}}^*$, an absolute value of the structure factor is the same for both stars and thus has tenfold rotational symmetry.

Electric field $\boldsymbol{E}$ satisfies the wave equation

$$\text{rot rot}\,\boldsymbol{E}(\boldsymbol{r}) = \left(\frac{\omega}{c}\right)^2\boldsymbol{D}(\boldsymbol{r}), \qquad (2)$$

where the displacement vector $\boldsymbol{D}(\boldsymbol{r}) = \varepsilon_b\boldsymbol{E}(\boldsymbol{r}) + 4\pi\boldsymbol{P}_{\text{exc}}(\boldsymbol{r})$ includes a nonresonant contribution, characterized by background dielectric constant $\varepsilon_b$, and excitonic polarization $\boldsymbol{P}_{\text{exc}}$.

 

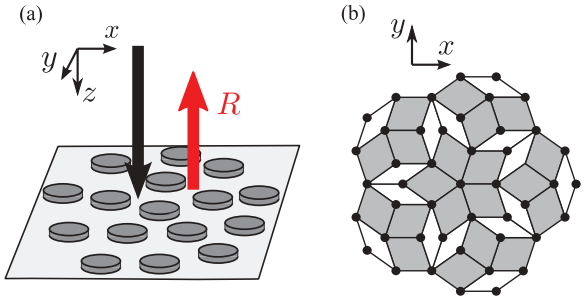


FIG. 1. (Color online) (a) Schematic illustration of light reflection from Penrose tiling of quantum dots. (b) Canonic Penrose tiling.

The material relation between the excitonic polarization and the electric field reads[14]

$$4\pi \boldsymbol{P}_{\rm exc}(\boldsymbol{r}) = T(\omega) \sum_{\boldsymbol{a}} \Phi(\boldsymbol{r}-\boldsymbol{a}) \int d^3r' \Phi(\boldsymbol{r}'-\boldsymbol{a}) \boldsymbol{E}(\boldsymbol{r}'), \tag{3}$$

where the resonant factor $T(\omega)$ is given by

$$T(\omega) = \frac{\pi \varepsilon_b a_{\rm B}^3 \omega_{\rm LT}}{\omega_0 - \omega - i\Gamma}. \tag{4}$$

Equation (3) contains summation over all dots, centered at the points $\boldsymbol{a}$ and characterized by excitonic envelope functions $\Phi(\boldsymbol{r}-\boldsymbol{a})$. Other excitonic parameters in Eq. (4) are as follows: longitudinal-transverse splitting $\omega_{\rm LT}$ and Bohr radius in the corresponding bulk semiconductor $a_{\rm B}$, resonance frequency $\omega_0$, and phenomenological nonradiative damping $\Gamma$. In the following calculations the excitonic envelope function is taken in the Gaussian form $\Phi(r) = \Phi_0 (\pi R)^{-3/2} \exp(-r^2/R^2)$, where $R$ is the characteristic radius of the quantum dot. For a $1s$ exciton, quantized in a parabolic potential as a whole, one has[14]

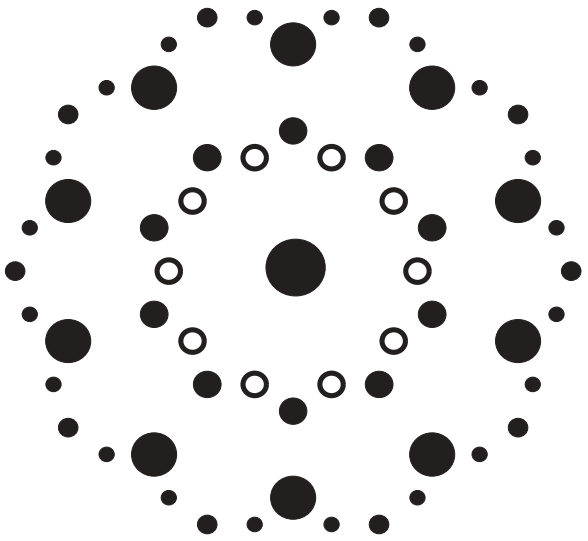

FIG. 2. Calculated diffraction image of Penrose tiling. The diameter of each spot, located at the point corresponding to the Bragg diffraction vector $\boldsymbol{G}$, is proportional to the absolute value of the structure factor $|f_{\boldsymbol{G}}|$. Only the spots with $|f_{\boldsymbol{G}}| > 0.15$ are shown. Empty spots correspond to diffraction vector with length $G^* \approx (2\pi/a_r) \times 1.05$, where $a_r$ is the side of the rhombus in Penrose tiling.

$\Phi_0 = 2^{-3/2}/\sqrt{\pi a_{\rm B}^3}$. The results weakly depend on the details of the shape of the envelope function for quantum dots that are small compared to the light wavelength. For instance, similar equations can be applied to the cluster of small metallic spheres with the radius $R \ll 2\pi c/\omega\sqrt{\varepsilon_b}$. In this case the functions $\Phi(r)$ are constant for $r < R$ and zero for $r \geqslant R$, and the factor $T(\omega)$ should be replaced by the resonant susceptibility of the metallic sphere near a given plasmon resonance.

Our calculation approach generalizes the methods used in Refs. 15 and 16. Electric field dependence on the coordinates $x$ and $y$ is described in the basis of plane waves. Different plane waves are coupled due to the Bragg diffraction. Coupling strength is determined by the structure factor coefficients. We keep in the plane wave expansions only 61 diffraction vectors $\boldsymbol{G}$ with the largest values of $f_{\boldsymbol{G}}$, shown in Fig. 2. Substituting Eq. (3) into Eq. (2) and applying Fourier transformation $\boldsymbol{E}_{\boldsymbol{k}} = \int d^3r \exp(-i\boldsymbol{k}\boldsymbol{r})\boldsymbol{E}(\boldsymbol{r})$ we obtain a closed equation for the electric field:

$$\boldsymbol{E}_{\boldsymbol{k}} = \frac{T(\omega)\Phi_k \hat{U}_{\boldsymbol{k}}}{k^2 - q^2} \sum_{\boldsymbol{a}} e^{-i\boldsymbol{k}\boldsymbol{a}} \int \frac{d^3k'}{(2\pi)^3} e^{i\boldsymbol{k}'\boldsymbol{a}} \Phi_{k'} \boldsymbol{E}_{\boldsymbol{k}'} + \boldsymbol{E}_{\boldsymbol{k}}^{(0)}. \tag{5}$$

Here $q = \omega\sqrt{\varepsilon_b}/c$, $\Phi_k = \Phi_0 \exp(-R^2k^2/4)$ is the excitonic envelope in $\boldsymbol{k}$ space, and the matrix $\hat{U}_{\boldsymbol{k}}$ is defined by

$$[U_{\boldsymbol{k}}]_{\alpha\beta} = \delta_{\alpha\beta} - \frac{k_\alpha k_\beta}{q^2}.$$

The inhomogeneous term $\boldsymbol{E}_{\boldsymbol{k}}^{(0)}$ in Eq. (5) describes the incident wave. We will distinguish in-plane and perpendicular components of all vectors and use the notation $\boldsymbol{Q} = (\boldsymbol{Q}_\parallel, Q_z)$, $\boldsymbol{Q}_\parallel = (Q_x, Q_y)$. Introducing the structure factor

$$\sum_{\boldsymbol{a}} e^{i(\boldsymbol{k}-\boldsymbol{k}')\boldsymbol{a}} = \frac{(2\pi)^2}{\bar{S}} \sum_{\boldsymbol{G}} \delta(\boldsymbol{k}_\parallel - \boldsymbol{k}'_\parallel - \boldsymbol{G}) f_{\boldsymbol{G}}, \tag{6}$$

where $\bar{S} \approx 0.81 a_r^2$ is the mean area per lattice site in the Penrose tiling,[13] we obtain

$$\boldsymbol{E}_{\boldsymbol{k}_\parallel+\boldsymbol{G},k_z} = \frac{T(\omega)\hat{U}_{\boldsymbol{k}_\parallel+\boldsymbol{G},k_z}\Phi_{\boldsymbol{k}_\parallel+\boldsymbol{G},k_z}}{(\boldsymbol{k}_\parallel+\boldsymbol{G})^2 + k_z^2 - q^2} \int \frac{dk'_z}{2\pi\bar{S}} \sum_{\boldsymbol{G}'} f_{\boldsymbol{G}-\boldsymbol{G}'} \times \Phi_{\boldsymbol{k}_\parallel+\boldsymbol{G}',k_z} \boldsymbol{E}_{\boldsymbol{k}_\parallel+\boldsymbol{G}',k'_z} + \boldsymbol{E}^{(0)}_{\boldsymbol{k}_\parallel+\boldsymbol{G},k_z}. \tag{7}$$

From now on, we restrict consideration to the case of normal incidence, $\boldsymbol{E}^{(0)}(\boldsymbol{r}) = \boldsymbol{e}_0 \exp(iqz)$ and $k_\parallel = 0$. To solve Eq. (7), we multiply each equation by $\Phi_{\boldsymbol{G},k_z}$ and integrate over $k_z$. This procedure leads to the following linear equations

$$\boldsymbol{\Lambda}_{\boldsymbol{G}} = i\chi L_{\boldsymbol{G}} \hat{U}_{\boldsymbol{G}} \sum_{\boldsymbol{G}'} f_{\boldsymbol{G}-\boldsymbol{G}'} \boldsymbol{\Lambda}_{\boldsymbol{G}'} + \delta_{\boldsymbol{G},0}\boldsymbol{e}_0 \tag{8}$$

for in-plane vectors

$$\boldsymbol{\Lambda}_{\boldsymbol{G}} = \frac{1}{\Phi_q} \int dk_z \Phi_{\boldsymbol{G},k_z} \boldsymbol{E}_{\boldsymbol{G},k_z}, \tag{9}$$

determining the Fourier components of electric field. Other quantities in Eq. (8) are the dimensionless susceptibility

$$\chi = \frac{\Gamma_0}{\omega_0 - \omega - i\Gamma}, \quad \Gamma_0 = \frac{\pi q a_B^3 \omega_{\rm LT} (\Phi_0)^2 e^{-(qR)^2/2}}{2\bar{S}},$$

and complex coefficients

$$L_G = \frac{q}{q_G}\mathrm{erfc}\left(\frac{iq_G R}{\sqrt{2}}\right), \quad q_G = \sqrt{q^2 - G^2}. \tag{10}$$

The complementary error function in Eq. (10) is defined as

$$\mathrm{erfc}(x) = 1 - \frac{2}{\sqrt{\pi}}\int_0^x \exp(-t^2)dt.$$

We note, that since $\mathrm{erfc}(x)$ vanishes with asymptotics $\exp(-x^2)/(\sqrt{\pi}x)$ at $x \to \infty$, both quantities $L_G$ and $\mathbf{\Lambda}_G$ quickly decay at $G \gtrsim 1/R$, ensuring the convergence of the sum over $G'$ in Eq. (8).

After the vectors $\mathbf{\Lambda}_G$ are found from system (8), the electric field is found by substitution of Eq. (9) into Eq. (7). At the large distances from the plane with quantum dots ($|z| \gg R, 1/q$) the field can be presented as

$$\boldsymbol{E}(\boldsymbol{r}) = \sum_{\boldsymbol{G}} e^{i\boldsymbol{G}\boldsymbol{\rho}} \times \begin{cases} e^{-iq_G z}\boldsymbol{E}_{\boldsymbol{G}}^{(r)}, & (z \to -\infty), \\ e^{iq_G z}\boldsymbol{E}_{\boldsymbol{G}}^{(t)}, & (z \to +\infty), \end{cases}$$

where $\boldsymbol{\rho} = (x, y)$ and the vectors $\boldsymbol{E}_{\boldsymbol{G}}^{(r)}$ and $\boldsymbol{E}_{\boldsymbol{G}}^{(t)}$ determine the amplitudes of the reflected and transmitted waves, respectively. In particular, we get

$$\boldsymbol{E}_{\boldsymbol{G}}^{(r)} e^{-iq_G z} = T(\omega)\int \frac{dk_z}{2\pi}\Phi_q \Phi_{\boldsymbol{G},k_z}\frac{e^{ik_z z}\hat{U}_{\boldsymbol{G},k_z}}{k_z^2 - q^2} \times \sum_{\boldsymbol{G}'} f_{\boldsymbol{G}-\boldsymbol{G}'}\mathbf{\Lambda}_{\boldsymbol{G}'}, \quad (z \to -\infty), \tag{11}$$

and a similar expression for $\boldsymbol{E}_{\boldsymbol{G}}^{(t)}$. The result reads

$$\boldsymbol{E}_{\boldsymbol{G}}^{(r)} = \hat{U}_{\boldsymbol{G},q_G}\boldsymbol{S}_{\boldsymbol{G}}, \quad \boldsymbol{E}_{\boldsymbol{G}}^{(t)} = \boldsymbol{e}_0\delta_{G,0} + \hat{U}_{\boldsymbol{G},-q_G}\boldsymbol{S}_{\boldsymbol{G}}, \tag{12}$$

$$\boldsymbol{S}_{\boldsymbol{G}} = i\chi\frac{q}{q_G}\sum_{\boldsymbol{G}'} f_{\boldsymbol{G}-\boldsymbol{G}'}\mathbf{\Lambda}_{\boldsymbol{G}'}. \tag{13}$$

Thus, the specular reflection coefficient is given by $R(\omega) = |S_0|^2$. Due to the fivefold rotational symmetry of the Penrose tiling, the reflected wave amplitude $\boldsymbol{S}_0$ is parallel to $\boldsymbol{e}_0$, and its magnitude is independent of the orientation of $\boldsymbol{e}_0$. We note that for zero exciton nonradiative decay ($\Gamma = 0$), the energy flux conservation condition along the $z$ direction holds, i.e.,

$$|S_0|^2 + |1 + S_0|^2 + 2\sum_{0<G<q}\frac{q_G}{q}\left[|\boldsymbol{S}_{\boldsymbol{G}}|^2 - \frac{|\boldsymbol{G}\boldsymbol{S}_{\boldsymbol{G}}|^2}{q^2}\right] = 1, \tag{14}$$

where three terms in the left-hand side correspond to specularly reflected, transmitted, and diffracted waves, respectively. Equation (14) can be rigorously derived from Eqs. (8)–(13) taking into account that $\mathrm{Re}\, L_G = q/q_G$ for $G < q$.

Reflection coefficient $r(\omega) \equiv S_0(\omega)$ has a simple analytic form only if the in-plane diffraction is totally neglected, i.e., only one vector $G = 0$ is included in the plane wave expansions of Eqs. (7) and (8). The result reads

$$r(\omega) = \frac{i\Gamma_0}{\tilde{\omega}_0 - \omega - i(\Gamma + \Gamma_0)}, \tag{15}$$

where

$$\tilde{\omega}_0 = \omega_0 + \Gamma_0\,\mathrm{Im}\,\mathrm{erfc}\left[\frac{iq(\omega_0)R}{\sqrt{2}}\right]. \tag{16}$$

Thus, the quantity $\Gamma_0$ can be interpreted as exciton radiative decay (evaluated neglecting diffraction), while $\tilde{\omega}_0$ is the exciton resonance frequency renormalized by the interaction with light. In Eq. (16) we have neglected the frequency dependence of the argument of the error function; it is evaluated at $\omega = \omega_0$. Equation (15) is similar to the reflection coefficient from the quantum-well exciton resonance.[14] It is valid only if inter-dot distances are small compared to the light wavelength, $a_r \ll 2\pi/q$. If $a_r \gtrsim 2\pi/q$, the in-plane diffraction must be included into theoretical consideration. Generally it can be done only numerically. The analytical expression for the reflection coefficient, obtained taking into account the diffraction vector $G = 0$ and the star of given diffraction vector $\boldsymbol{G}$, is presented in the next section. We note, that although experimental realization of the coupling between spatially separated quantum dots via an electromagnetic field is a challenging task, substantial progress has been recently achieved for dots in the microcavities.[17,18]

## III. REFLECTION COEFFICIENT IN THE TWO-STAR APPROXIMATION

In this section we consider general quasicrystalline tiling with $N$-fold rotational symmetry. The specular reflection coefficient of the normally incident light is calculated analytically. We take into account $N + 1$ diffraction vectors, belonging to the two stars, namely, the trivial star with single vector $\boldsymbol{G} = 0$ and the star of the given vector $G^*$, including $N$ diffraction vectors

$$\boldsymbol{G}_n = G^*(\cos n\varphi, \sin n\varphi), \tag{17}$$

where $n = 1, \ldots, N$ and $\varphi = 2\pi/N$. Coupling between plane waves corresponding to $G = 0$ and $\boldsymbol{G} = \boldsymbol{G}_n$ is described by the structure factor coefficient $f_{G^*}$. It is also essential to consider the coupling between the wave vectors within the star of vector $G^*$. This coupling is characterized by structure factor coefficients

$$f_m \equiv f_{\boldsymbol{G}_{m+n}-\boldsymbol{G}_n}, \tag{18}$$

and shown for a Penrose tiling (where $N = 5$) in Fig. 2(b). Solid and dashed lines correspond to two possible values of coupling coefficients $f_m$. Under normal incidence of the wave $\boldsymbol{e}_0\exp(iqz)$, all vectors $\mathbf{\Lambda}$ lie in the $xy$ plane. Thus, Eqs. (8) are reduced to

$$\mathbf{\Lambda}_n = i\chi L_{G^*}\hat{U}_{\boldsymbol{G}_n}\left(\sum_{m=0}^{N-1} f_m\mathbf{\Lambda}_{m+n} + f_{G^*}\mathbf{\Lambda}_0\right), \tag{19}$$

$$\mathbf{\Lambda}_0 = i\chi L_0 f_{G^*}^*\sum_{n=1}^{N}\mathbf{\Lambda}_n + \boldsymbol{e}_0, \tag{20}$$

where $\mathbf{\Lambda}_n \equiv \mathbf{\Lambda}_{\boldsymbol{G}_n}$ for $n = 1, \ldots, N$. The system (8) includes $2(N + 1)$ linear equations for the Cartesian components of the vectors $\mathbf{\Lambda}$. To solve it, we use the $C_{Nv}$ symmetry of the problem. The solutions of Eqs. (19) and (20) can be sought in the form

$$\mathbf{\Lambda}_0 = \Lambda_0\boldsymbol{e}_0, \tag{21}$$

and

$$\begin{pmatrix}\Lambda_{n,x}\\ \Lambda_{n,y}\end{pmatrix} = C_0\begin{pmatrix}e_{0,x}\\ e_{0,y}\end{pmatrix} + C_2\begin{pmatrix}\cos(2n\varphi)e_{0,x} & +\sin(2n\varphi)e_{0,y}\\ -\cos(2n\varphi)e_{0,y} & +\sin(2n\varphi)e_{0,x}\end{pmatrix}. \quad (22)$$

The vector $\mathbf{\Lambda}_0$ in Eq. (21) is parallel to $\boldsymbol{e}_0$ and its magnitude is independent of polarization. The structure of Eq. (22) is more complex. Let us examine it for the $C_{5v}$ point symmetry group[19] of the Penrose tiling. Both terms in Eq. (22) are transformed by symmetry operations like vectors, and belong to the irreducible representation $E_1$. They stem from the direct product $D \times E_1$, where $D = A_1 + E_1 + E_2$ is a reducible representation describing the transformation of functions $\delta(\boldsymbol{k}_\parallel - \boldsymbol{G}_n)$, and the representation $E_1$ describes the transformation of the polarization vector components $e_{0,x}$ and $e_{0,y}$. First and second terms in Eq. (22) originate from the invariant $A_1$ and irreducible representation $E_2$ contained in $D$, respectively.

The set of vectors $\mathbf{\Lambda}$ in Eqs. (19) and (20) is characterized only by three unknown coefficients $\Lambda_0, C_0, C_2$. From Eq. (19) we find that

$$\frac{C_0}{C_2} = \frac{1+\eta-2\eta(A-B)}{\eta-1}, \quad \frac{C_0}{\Lambda_0} = \frac{\mathcal{G}}{Nf^*_{G^*}}, \quad (23)$$

where $\eta = 1 - G^2/q^2$,

$$A = i\chi L_{G^*}\sum_{m=0}^{N-1} f_m \cos^2 m\varphi, \quad B = i\chi L_{G^*}\sum_{m=0}^{N-1} f_m \sin^2 m\varphi,$$

and

$$\mathcal{G} = \frac{iN\chi L_{G^*}|f_{G^*}|^2}{2}\frac{1+\eta-2\eta(A-B)}{1-(\eta+1)A+\eta(A^2-B^2)}. \quad (24)$$

Making use of the second part of Eq. (23) in Eq. (20), we find

$$\Lambda_0 = \frac{1}{1-i\chi L_0\mathcal{G}}.$$

The reflection coefficient $r(\omega) \equiv \boldsymbol{e}_0 \cdot \boldsymbol{S}_0$ is found from Eq. (13):

$$r(\omega) = i\chi\boldsymbol{e}_0 \cdot \left(\mathbf{\Lambda}_0 + f^*_{G^*}\sum_{n=1}^{N}\mathbf{\Lambda}_n\right) \equiv i\chi(\Lambda_0 + Nf^*_{G^*}C_0). \quad (25)$$

The final expression for the reflection coefficient reads

$$r(\omega) = \frac{i\Gamma_0[1+\mathcal{G}(\omega)]}{\omega_0 - i\Gamma - i\Gamma_0 L_0[1+\mathcal{G}(\omega)] - \omega}. \quad (26)$$

The coefficient $\mathcal{G}$ represents the effect of in-plane diffraction on the specular reflection coefficient; at $\mathcal{G} = 0$, Eq. (26) reduces to Eq. (15). Expression (24) can be simplified for the Bragg structure with $q(\omega_0) = G^*$. In this case the coefficient $\eta$ can be neglected and

$$\mathcal{G} = \frac{iN\chi L_{G^*}|f_{G^*}|^2}{2(1-A)}.$$

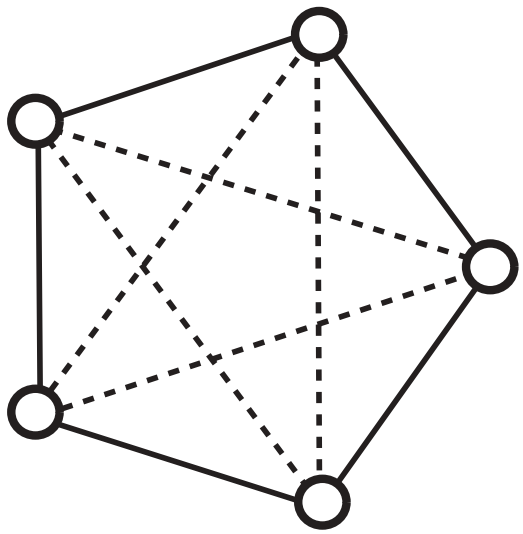

FIG. 3. Schematic illustration of the coupling between five wave vectors of the star $G^*\boldsymbol{e}_n$ in the Penrose tiling due to Bragg diffraction.

Moreover, near the Bragg resonance the function $L_{G^*}(\omega)$ can be approximated by the following expression

$$L_{G^*} \approx \sqrt{\frac{\omega_0}{2(\omega-\omega_0)}}. \quad (27)$$

We note, that for odd number $N$ of vectors in a star we have to include in the analytical calculation also the set of vectors

$$\boldsymbol{G}^-_n = -G^*(\cos n\varphi, \sin n\varphi), \quad (28)$$

opposite to the vectors $\boldsymbol{G}_n$ in Eq. (17). For the Penrose tiling, where $N = 5$, it turns out that the two stars (17) and (28) are not coupled by diffraction and interact independently with the wave $G = 0$. Absolute values of the structure factor coefficients are the same for both stars. Thus, the two-star approximation Eq. (17) can be easily extended to include three stars with $2N + 1$ diffraction vectors by making the replacement $\mathcal{G} \to 2\mathcal{G}$ in Eq. (26):

$$r(\omega) = \frac{i\Gamma_0[1+2\mathcal{G}(\omega)]}{\omega_0 - i\Gamma - i\Gamma_0 L_0[1+2\mathcal{G}(\omega)] - \omega}. \quad (29)$$

For Penrose tiling the values of structure factors corresponding to $G^* = 4\pi\tau^2/(5a_r) \approx 1.05 \times 2\pi/a_r$ are $|f_{G^*}| = 0.38$, $f_{\pm1} = 0.47$ (solid lines in Fig. 3), $f_{\pm2} = 0.76$ (dashed lines in Fig. 3).

## IV. RESULTS AND DISCUSSION

In this section we analyze light reflection from periodic and quasicrystalline lattices. Before considering the quasicrystalline case, it is instructive to examine the periodic lattice of quantum dots. To test Eq. (26) we focus on quadratic lattice analyzed in Ref. 15. In this case $f_m = f_{G^*} = 1$ and $A = B = (N/2)\chi L_{G^*}$, where $N$ equals 4 or 8 depending on the value of $G^*$. Thus, we get

$$\mathcal{G} = \frac{iN\chi L_{G^*}[1-(G^*)^2/2q^2]}{1-iN\chi L_{G^*}[1-(G^*)^2/2q^2]},$$

and

$$r_{\rm per}(\omega) = \frac{i\Gamma_0}{\omega_0 - i\Gamma_0\{L_0 + NL_{G^*}[1-(G^*)^2/2q^2]\} - i\Gamma - \omega}, \tag{30}$$

in agreement with Ref. 15. This expression has a pole at the frequency determined by the sum of contributions of the stars, corresponding to the vectors $G = 0$ and $G = G^*$. The reflection spectrum $R(\omega)$ from the periodic Bragg structure where

$$\omega_0 = \omega_{G^*} \equiv cG^*/n_b \tag{31}$$

is illustrated by dashed curves in Figs. 4(a) and 4(b). We stress that in Eq. (30) it is important to take into account the singular dependence of $L_{G^*}$ on $\omega$, which is approximately described by Eq. (27). Substituting Eq. (27) into Eq. (30) we obtain a simple result for the reflection coefficient from the periodic structure:

$$r_{\rm per}(\omega) \approx \frac{i\Gamma_0}{\omega_0 - \omega - i\Gamma - i\Gamma_0 L_0 - N\Gamma_0\sqrt{\frac{\omega_0}{8(\omega_0-\omega)}}}. \tag{32}$$

Equation (32) differs from Eq. (15) by the presence of the last term in the denominator. This term with the square root singularity leads to the standard Wood anomalies in periodic lattices.[7] However, it turns out that for the relatively weak quantum dot exciton resonances ($\Gamma_0/\omega_0 \ll 1$), the features due to this singularity are weakly resolved in the spectrum of the periodic structure. Indeed, the function $R(\omega) \equiv |r_{\rm per}(\omega)|^2$ has a maximum at

$$\omega_1 \approx \omega_0 - \Gamma_0\left(\frac{N^2\omega_0}{8\Gamma_0}\right)^{1/3}, \quad R(\omega_1) \approx \left(\frac{\Gamma_0}{\Gamma_0+\Gamma}\right)^2, \tag{33}$$

then turns to zero at $\omega = \omega_0$ and has a second maximum at

$$\omega_2 \approx \omega_0 + \Gamma_0\left(\frac{N^2\omega_0}{16\Gamma_0}\right)^{1/3}, \quad R(\omega_2) \approx \frac{4^{4/3}}{5N^{4/3}}\left(\frac{\omega_0}{\Gamma_0}\right)^{-2/3}, \tag{34}$$

see dashed curves in Fig. 4. The characteristic notch at $\omega = \omega_0$ between the two maxima at $\omega_1$ and $\omega_2$ represents the Wood anomaly in the optical spectrum. Since $R(\omega_1) \gg R(\omega_2)$, this notch is manifested only in logarithmic scale, see Fig. 4(b). In the linear scale of Fig. 4(a), only one Lorentzian peak is resolved in the reflection spectrum at $\omega_1 \approx \omega_0 - 12\Gamma_0$. The red shift $\omega_0 - \omega_1$ of the peak frequency from the exciton resonance is due to radiative corrections. The absolute value of the shift is large compared to $\Gamma_0$, because the structure is tuned to the Bragg condition (31).

We now proceed to the quasicrystalline case. Dotted curves in Fig. 4(a) and Fig. 4(b) depict analytical result (26) for a Penrose tiling, tuned to the Bragg resonance (31) at the diffraction vector $|\boldsymbol{G}| \equiv G^* = 4\pi\tau^2/(5a_r)$. The spectrum was calculated using Eq. (29) and taking into account the diffraction vector $G = 0$ and ten vectors $\pm G^*\boldsymbol{e}_n$, belonging to two opposite stars; see empty spots in Fig. 2.

In the quasicrystalline system, Eqs. (24) and (29) for the reflection coefficient are more complex than in the periodic case. To find the positions of the maxima and minima of the reflection coefficient $|r(\omega)|^2$, one has to solve quintic equations, so it is impossible to generalize Eqs. (33) and (34) directly. However, the calculation clearly demonstrates that the spectrum for the Penrose tiling remarkably differs from that in the periodic case. Comparing dashed and dotted curves in Fig. 4(a), we conclude that the single peak at $\omega \approx \omega_1$, given by Eq. (33) is transformed in a quasicrystal into two distinct peaks at $\omega \approx \omega - 12\Gamma_0$ and $\omega \approx \omega - \Gamma_0$. The dotted curve has also a dip with $R = 0$ at $\omega \approx \omega_0 - 9\Gamma_0$, revealed in the logarithmic scale of Fig. 4(b). This dip is analogous to the Wood anomaly in the periodic case at $\omega = \omega_0$. However, the dip frequency is shifted from $\omega_0$. Therefore, it is not given by the condition of diffraction channel opening $q(\omega_0) = G^*$, as in the periodic structure.

The results of numerical calculation for the Penrose tiling, including 61 diffraction vectors from Fig. 2(a), are shown by the solid curve in Fig. 4. Comparing solid and dotted curves, we see that the spectrum is well described by the analytical approximation (29). Indeed, since the structure is tuned to the specific Bragg resonance (31), the spectrum does not change considerably when extra diffraction vectors with $G \neq 0$, $G \neq G^*$ are taken into account. The solid curve has only a narrow additional dip at the right wing of the peak at $\omega \approx \omega_0$.

We conclude from Fig. 4 that the reflectivity from the quasicrystalline lattice tuned to the grating resonance differs from that from the periodic one by (i) the shift of the position of the notch where $R(\omega) = 0$ and (ii) the presence of a second distinct peak in the spectrum. The magnitude of the

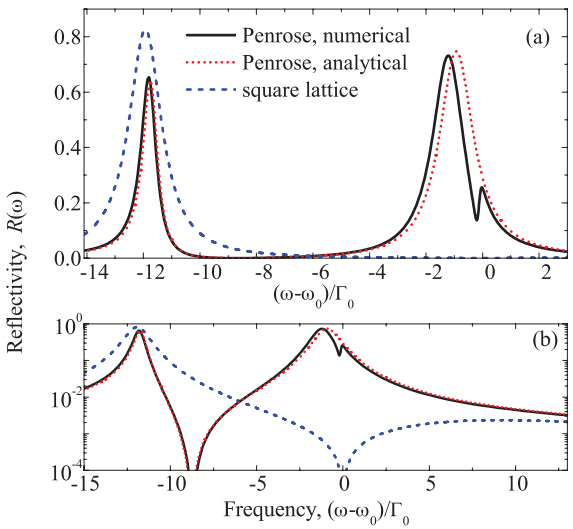


FIG. 4. (Color online) (a) Specular reflection coefficient $R(\omega)$ from a Penrose quasicrystal tuned to the Bragg condition $\omega_{G^*} = \omega_0$. (b) Same curves as in (a) but in a semilogarithmic scale. Calculation was performed for the following set of parameters: $\Gamma_0/\omega_0 = 10^{-3}$, $\Gamma/\Gamma_0 = 0.1$, $R/a_r = 0.2$. Solid curve presents numerical calculation including all diffraction vectors from Fig. 2, while dotted curve is the analytical result (29), obtained including 11 vectors. Dashed curve corresponds to the reflection coefficient from a periodic square lattice, Eq. (30), where $N = 4$. Other parameters are indicated in text.

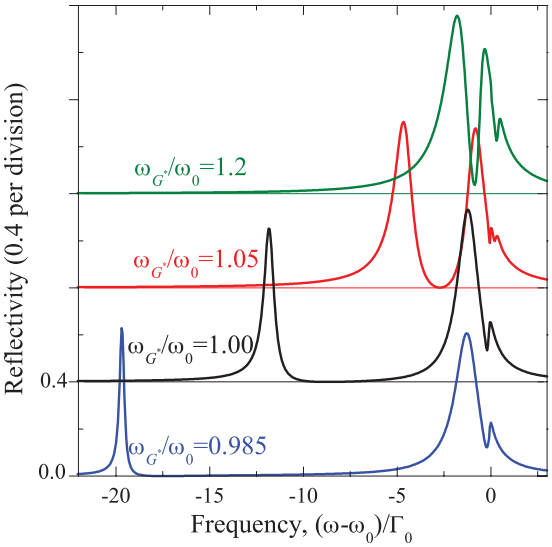


FIG. 5. (Color online) Specular reflection coefficient from Penrose quasicrystals with different lattice constants $a_r$, calculated for $\omega_{G^*}/\omega_0 = 0.985, 1, 1.05, 1.2$. For better presentation, each following curve is shifted upward by 0.4 from the preceding one. Horizontal lines mark corresponding zero levels. Other parameters are the same as in Fig. 4.

splitting between the two peaks in the reflectivity spectrum of the quasicrystal is on the order of $\Gamma_0(\omega_0/\Gamma_0)^{1/3}$ and can considerably exceed $\Gamma_0$. We interpret the two-peak spectral shape as a Wood anomaly, emerging due to the quasicrystalline order. Such spectral structure may be also observed in a slightly distorted 2D periodic resonant structure[16] and in 2D resonant photonic crystals with a compound elementary supercell.[20] To obtain the spectra with the shape similar to the solid and dotted curves in Fig. 4 it suffices to tune the structure to the Bragg condition with the structure factor coefficient large but less than unity.

Figure 5 illustrates the effect of detuning from the resonant Bragg condition (31). One can see that the splitting between the two peaks increases with detuning for $\omega_{G^*} < \omega_0$. The low-frequency peak becomes sharper and its position for the large detuning, $|\omega_0 - \omega_{G^*}| \gg \Gamma_0(\omega_0/\Gamma_0)^{1/3}$, is close to $\omega_{G^*}$. For $\omega_{G^*} > \omega_0$ the value of the splitting decreases. With the further increase of detuning the two peaks merge into one peak with structured dips, similar to what occurs in the one-dimensional Fibonacci multiple quantum wells.[21] The qualitative difference between spectral shapes for $\omega_{G^*} < \omega_0$ and $\omega_{G^*} > \omega_0$, revealed in Fig. 5, can be understood taking into account that the diffraction channel with $G = G^*$ is closed for $\omega_{G^*} > \omega_0$, i.e., the corresponding wave $\exp(iq_{G^*}|z|)$ is evanescent.

## V. CONCLUSIONS

To summarize, we have developed a theory of light diffraction on the 2D quasicrystalline planar array of quantum dots. An analytic expression for specular reflection coefficient has been derived. While for the periodic lattice the specular reflection spectrum has a single distinct peak near the exciton resonance frequency, for the quasicrystalline lattice the spectrum consists of two peaks. This two-peak structure of the spectrum is related to the interplay between specular reflection and in-plane light diffraction, and represents a lattice Wood anomaly, specific for the quasicrystalline structure. The reflection spectrum for the quasicrystalline lattice also has a notch with zero reflectivity, being a fingerprint of the Wood anomaly known in literature. However, contrary to the periodic case, the position of this notch does not correspond to the diffraction channel opening condition.

## VI. ACKNOWLEDGMENT

It is a great pleasure to thank E. L. Ivchenko for numerous illuminating discussions. Support by the RFBR and "Dynasty" Foundation – ICFPM is gratefully acknowledged.

*poddubny@coherent.ioffe.ru

[1] D. Levine and P. J. Steinhardt, Phys. Rev. Lett. **53**, 2477 (1984).
[2] A. N. Poddubny and E. L. Ivchenko, Physica E **42**, 1871 (2010).
[3] D. Goldberg, L. I. Deych, A. A. Lisyansky, Z. Shi, V. M. Menon, V. Tokranov, M. Yakimov, and S. Oktyabrsky, Nat. Photonics **3**, 662 (2009).
[4] J. Hendrickson, B. C. Richards, J. Sweet, G. Khitrova, A. N. Poddubny, E. L. Ivchenko, M. Wegener, and H. M. Gibbs, Opt. Express **16**, 15382 (2008).
[5] A. Gopinath, S. V. Boriskina, B. M. Reinhard, and L. Dal Negro, Opt. Express **17**, 3741 (2009).
[6] A. Hessel and A. A. Oliner, Appl. Opt. **4**, 1275 (1965).
[7] N. García and A. Maradudin, Opt. Commun. **45**, 301 (1983).
[8] N. A. Gippius, S. G. Tikhodeev, and T. Ishihara, Phys. Rev. B **72**, 045138 (2005).
[9] A. Tikhonov, J. Bohn, and S. A. Asher, Phys. Rev. B **80**, 235125 (2009).
[10] N. Papasimakis, V. A. Fedotov, A. S. Schwanecke, N. I. Zheludev, and F. J. García de Abajo, Appl. Phys. Lett. **91**, 081503 (2007).
[11] M. A. Kaliteevski, S. Brand, R. A. Abram, T. F. Krauss, P. Millar, and R. M. DeLa Rue, J. Phys.: Condens. Matter **13**, 10459 (2001).
[12] J. E. S. Socolar, P. J. Steinhardt, and D. Levine, Phys. Rev. B **32**, 5547 (1985).
[13] W. Steurera and T. Haibacha, in *International Tables for Crystallography* (Wiley, New York, 2006), Vol. B, Chap. 4.6.
[14] E. L. Ivchenko, *Optical Spectroscopy of Semiconductor Nanostructures* (Alpha Science International, Harrow, UK, 2005).
[15] E. L. Ivchenko, Y. Fu, and M. Willander, Phys. Solid State **42**, 1756 (2000).
[16] A. N. Poddubny, L. Pilozzi, M. M. Voronov, and E. L. Ivchenko, Phys. Rev. B **80**, 115314 (2009).

[17] A. Laucht, J. M. Villas-Bôas, S. Stobbe, N. Hauke, F. Hofbauer, G. Böhm, P. Lodahl, M.-C. Amann, M. Kaniber, and J. J. Finley, Phys. Rev. B **82**, 075305 (2010).

[18] E. Gallardo, L. J. Martínez, A. K. Nowak, D. Sarkar, H. P. van der Meulen, J. M. Calleja, C. Tejedor, I. Prieto, D. Granados, A. G. Taboada, J. M. García, and P. A. Postigo, Phys. Rev. B **81**, 193301 (2010).

[19] M. S. Dresselhaus, G. Dresselhaus, and A. Jorio, *Group Theory: Application to the Physics of Condensed Matter* (Springer, New York, 2008).

[20] E. L. Ivchenko, M. M. Voronov, M. V. Erementchouk, L. I. Deych, and A. A. Lisyansky, Phys. Rev. B **70**, 195106 (2004).

[21] A. N. Poddubny, L. Pilozzi, M. M. Voronov, and E. L. Ivchenko, Phys. Rev. B **77**, 113306 (2008).